



## Search for $W'$ -like Resonances Decaying to a Top and a Bottom Quark in the Missing Transverse Energy plus Jets Final State

The CDF Collaboration  
URL <http://www-cdf.fnal.gov>  
(Dated: 2014-02-13)

This Note reports on a search for  $W'$ -like resonances decaying to  $tb$  in the full data set of proton-antiproton collisions at  $\sqrt{s} = 1.96$  TeV recorded by the CDF II detector at the Tevatron, corresponding to an integrated luminosity of  $9.1 \text{ fb}^{-1}$ . We consider events having no identified charged lepton, a transverse energy imbalance, and two or three jets, of which at least one is consistent with originating from the decay of a  $b$  quark. No significant excess above SM prediction is found. Using a benchmark  $W' \rightarrow tb$  left-right symmetric model, we place 95% CL upper limits on the  $W'$  production cross section times branching ratio to  $tb$ . Assuming a  $W'$  with SM-like couplings and decay to leptons allowed (forbidden), we exclude  $W' \rightarrow tb$  for  $W'$  masses below 820 (840)  $\text{GeV}/c^2$ . Relaxing the hypothesis on SM-like couplings, we exclude  $W'$  boson coupling strength values as a function of  $W'$  mass down to  $g_{W'} = 0.4g_{\text{SM}}$  for  $M_{W'} = 300 \text{ GeV}/c^2$ .

*Preliminary Results for Winter 2014 Conferences*

## I. INTRODUCTION

Several modifications of the Standard Model (SM) of particle physics include massive, short-lived states decaying to pairs of SM leptons or quarks. A resonance decaying to a top and a bottom quark  $tb$  (where  $tb$  indicates both the state  $t\bar{b}$  and its charge conjugate  $\bar{t}b$ ) can appear in models featuring one or more massive charged vector bosons, generically denoted as  $W'$ , such as  $SU(2)_R$  SM extensions [1], Kaluza-Klein extra-dimensions, [2, 3], technicolor [4, 5] or Little Higgs scenarios [6]. Searches for  $W'$  bosons in the  $W' \rightarrow tb$  decay channel are complementary to searches in the leptonic decay channel  $W' \rightarrow \ell\nu$ , and can probe cases where the couplings of the  $W'$  to fermions are free parameters, or the leptonic decay mode is suppressed or forbidden.

In the recent past, searches in the  $W' \rightarrow tb$  channel have been performed by the CDF [7] and DØ [8] experiments at the Tevatron, and by the ATLAS [9] and CMS [10] experiments at the LHC. For resonance searches at the highest masses, the LHC experiments have superior sensitivity to the Tevatron due to the higher center-of-mass energy. However, in the lower mass region ( $M_{W'} < 700 \text{ GeV}/c^2$ ) the Tevatron experiments have competitive sensitivity due to the more favorable signal-to-background ratio in searches for particles produced in quark-initiated states, such as the  $W'$ , with respect to the gluon-initiated dominant SM background processes.

In this Note, we present a new search for  $W'$ -like resonances decaying to  $tb$  in events where  $t \rightarrow Wb$  and the  $W$  decays to a charged lepton-neutrino pair, but either the lepton is a electron or muon which is not identified, or is a hadronically decaying  $\tau$  reconstructed as a jet. Events in this channel are characterized by the presence of significant transverse energy imbalance, two jets originated from  $b$ -quarks, and no identified charged leptons.

A simple left-right symmetric SM extension [11], predicting the existence of  $W'$  bosons of unknown mass and universal weak coupling strength to SM fermions, is used as a benchmark model. Since no specific assumptions on the signal model are made throughout the analysis, this search is sensitive to any narrow resonant state decaying to  $tb$ .

## II. EVENT PRESELECTION

The collision events discussed in this Note were produced at the Tevatron  $p\bar{p}$  collider at a center-of-mass energy of 1.96 TeV and were recorded by the CDF II detector [12, 13]. In this analysis the full CDF II data set is used, corresponding to an integrated luminosity of  $9.1 \text{ fb}^{-1}$ .

The selection criteria used for this search are similar to other CDF analyses with the same final-state signature [14]. The data were collected using online event selections (triggers) requiring either large  $\cancel{E}_T$ , or large  $\cancel{E}_T$  and at least two jet candidates. After event reconstruction, candidate events are selected by requiring  $\cancel{E}_T > 50 \text{ GeV}$ , and two high- $p_T$  jets [15] with transverse energies that satisfy  $E_T(j_1) > 25 \text{ GeV}$  and  $E_T(j_2) > 20 \text{ GeV}$ , respectively. In order to gain sensitivity in events where the  $\tau$  lepton in the  $t \rightarrow Wb \rightarrow \tau\nu b$  channel is reconstructed as a jet in the calorimeter, events with three jets are selected if the third-most energetic jet satisfies  $E_T(j_3) > 15 \text{ GeV}$ . To ensure that leading- $E_T$  jets  $j_1, j_2$  are within the silicon detector acceptance, they are required to satisfy  $|\eta(j_{1,2})| < 2$ , where at least one of them must satisfy  $|\eta(j_i)| < 0.9$ . Events are rejected if they contain a reconstructed electron or muon, or a number of reconstructed jets larger than 3, where each jet  $j_i$  exceeds the minimum transverse energy threshold ( $E_T > 15 \text{ GeV}$ ) and has pseudorapidity  $|\eta(j_i)| < 2.4$ .

In events where the large  $\cancel{E}_T$  is due to mismeasurement of jet energies, the  $\vec{\cancel{E}}_T$  is often aligned with the direction of the second-most energetic jet  $\vec{E}_T(j_2)$ . Such events are rejected by requiring  $\Delta\varphi(\vec{\cancel{E}}_T, \vec{E}_T(j_1)) \geq 1.5$  and  $\Delta\varphi(\vec{\cancel{E}}_T, \vec{E}_T(j_{2,3})) \geq 0.4$ . In order to identify jets as being originated from the fragmentation of a hadron containing a  $b$ -quark (“ $b$ -tagging”), two different algorithms are used: SecVTX [13] a tight (T) algorithm, and JetProb [16], a loose (L) algorithm. At least one of the leading jets is required to be tagged by SecVTX. Events are further divided among three statistically independent regions, depending on whether the other leading jet is not tagged (Exclusive 1 Tight, 1T), tagged by JetProb but not by SecVTX (1 Tight + 1 Loose, TL), and tagged by SecVTX (2 Tight, TT). This division results in an increased sensitivity because signal-to-noise ratio and background composition are different among the  $b$ -tagging subsamples. Events satisfying the aforementioned requirements comprise the *preselection* sample.

## III. SIGNAL AND BACKGROUND MODELING

The most important contribution to the preselection sample is due to multijet production from strong interactions (QCD multijet). Significant contributing processes include: top-antitop quark pair production ( $t\bar{t}$ ), electroweak single top production, dibosons ( $WW/WZ$ ), and production of jets in association with a  $W$  or  $Z$  boson ( $W/Z + \text{jets}$ ), including both heavy-flavor jets (from  $b$  or  $c$  quarks) and jets from light-flavor quarks which have been erroneously

$b$ -tagged. A combination of Monte Carlo simulations and data-driven techniques are used to derive the models for SM background processes. The ALPGEN generator [17] is used to simulate events for diboson and  $W/Z + \text{jets}$ ;  $t\bar{t}$  and single top are simulated with POWHEG [18]. Parton showering is performed by PYTHIA [19]. The event generation process includes a simulation of the detector response [20], and the resulting simulated event samples are subjected to the same reconstruction and analysis chain as the data. The normalization for  $t\bar{t}$ , single top, and diboson templates is constrained to the theoretical cross section value. The normalization for  $W/Z + \text{jets}$  templates is left unconstrained in the final fit procedure.

QCD multijet events are difficult to model with simulation. For this reason, a QCD multijet background model is derived from data in an independent data sample composed of events with  $\Delta\varphi(\vec{E}_T, \vec{E}_T^{j_2}) < 0.4$  and  $50 < E_T < 70$  GeV, consisting almost entirely of QCD multijet contributions. First, a probability density function  $f_i$  is formed separately in each  $b$ -tagging subsample  $i$  ( $i = 1\text{T}, \text{TL}, \text{TT}$ ) by taking the ratio between tagged and pretagged events as a function of several variables, as described in detail in [14]. Then, a QCD multijet template is determined separately for each region  $i$  by weighting the untagged data in the preselection sample according to the probability density functions  $f_i$ . To determine the appropriate normalization for a given category, a scale factor is derived in a different control region, defined below, where the tagged diboson, top and  $W/Z + \text{jets}$  background estimates are subtracted from the tagged data.

The signal model is a  $W'$  with purely right-handed decays, simulated using PYTHIA for  $W'$  mass  $M_{W'}$  hypotheses in the range  $200 \leq M_{W'} \leq 900$  GeV/ $c^2$  in 100 GeV/ $c^2$  increments. As the  $W'$  helicity does not affect analysis observables, this model is valid for both a right-handed and a left-handed  $W'$  under the assumption of no interference with SM  $W$  boson. Two different scenarios are considered, depending whether the leptonic decay mode  $W' \rightarrow \ell\nu$  is allowed or forbidden. The latter, for instance, is the case if the right-handed neutrino  $\nu_R$  is more massive than the  $W'$ . The only effect of the forbidden leptonic decay mode is an increased branching fraction  $\mathcal{B}(W' \rightarrow tb)$ .

#### IV. DISCRIMINANTS

As an intermediate background rejection step, an Artificial Neural Network,  $\text{NN}_{\text{QCD}}$ , is employed to further separate the dominant QCD multijet background from signal and other backgrounds.  $\text{NN}_{\text{QCD}}$  is a 13-variable feed-forward multilayer perceptron, bearing activity-derived ( $E_T, \cancel{p}_T$  [21]), angular ( $\Delta\varphi(\vec{E}_T, \vec{\cancel{p}}_T)$ , angular separations between  $\vec{E}_T$ ,  $\vec{\cancel{p}}_T$  and the jet directions), and event-shape (sphericity [22]) observables. Single top  $s$ -channel events from simulation are used as the signal sample in the training of  $\text{NN}_{\text{QCD}}$ . This choice exploits the similar final state topology and kinematical distributions between this process and the signal, while at the same time ensuring a consistent performance in QCD multijet background separation across the whole  $W'$  mass hypothesis range, as no information on the resonant  $W'$  mass is present in the training event sample, and no related bias is introduced in the training procedure.

Figure 1 shows the  $\text{NN}_{\text{QCD}}$  output distribution for events in the  $\text{TT}$  subsample. Only events with  $\text{NN}_{\text{QCD}} > 0.45$  are retained, forming the *signal* region. This prescription results in an increase in binned significance of about 50% for a 300 GeV/ $c^2$   $W'$ . The independent region  $\text{NN}_{\text{QCD}} < 0.1$  is composed almost entirely of QCD multijet events, and is used to derive the normalization for the QCD multijet background templates in the signal region. Table I shows expected event yields for background processes, observed data events, and expected number of events for one signal hypothesis.

The transverse invariant mass of the  $\cancel{E}_T$  and all jets,  $M_T(\cancel{E}_T, j_{1,2,3})$ , is used to discriminate the  $W' \rightarrow tb$  signal from the remaining backgrounds. This variable corresponds to the reconstructed transverse invariant mass of the  $W'$  in events where the jets originate from  $b$  quarks, and both the lepton and the neutrino originated from the  $W$  boson are not detected and contribute to the  $\cancel{E}_T$ . Figure 1 shows the  $M_T(\cancel{E}_T, j_{1,2,3})$  distribution for events in the  $\text{TT}$  subsample.

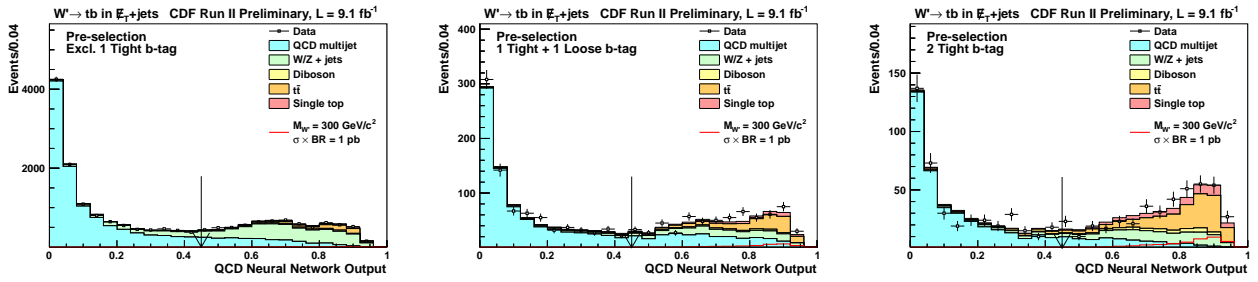


FIG. 1. Distribution of the QCD Neural Network in the pre-selection region in the subsample with exactly one tight  $b$ -tagged jet (left), one tight and one loose  $b$ -tagged jet (middle) and two tight  $b$ -tagged jets (right). Templates for background processes are normalized to their expected values. The expected distribution for a  $300 \text{ GeV}/c^2$   $W'$  with  $\sigma(p\bar{p} \rightarrow W') \times \mathcal{B}(W' \rightarrow tb) = 1 \text{ pb}$  is shown in red. The arrow at  $\text{NN}_{\text{QCD}} = 0.45$  marks the minimum requirement that defines the signal region.

	1T	TL	TT
QCD multijet	$1871 \pm 113$	$238 \pm 26$	$71 \pm 10$
$W/Z + \text{jets}$	$3757 \pm 647$	$137 \pm 25$	$94 \pm 17$
Diboson	$239 \pm 29$	$25 \pm 3$	$24 \pm 3$
$t\bar{t}$	$690 \pm 73$	$142 \pm 17$	$151 \pm 18$
Single top	$272 \pm 48$	$43 \pm 8$	$51 \pm 9$
Total Background	$6830 \pm 663$	$584 \pm 41$	$392 \pm 28$
Observed	6815	620	405
$M_{W'} = 300 \text{ GeV}$ ( $\sigma \times \mathcal{B} = 1 \text{ pb}$ )	$96 \pm 30$	$34 \pm 11$	$45 \pm 14$

TABLE I. Expected and observed event yields in signal region defined by the QCD Neural Network  $> 0.45$  requirement in the three subsamples with exactly one tight  $b$ -tagged jet (1T), one tight and one loose  $b$ -tagged jet (TL) and two tight  $b$ -tagged jets (TT). The uncertainties in the expected number of events are due to the uncertainties on the theoretical cross section and to the uncertainties on signal and background modeling. Templates for background processes are normalized to their expected values. Expected number of events for one choice of  $W'$  mass and  $\sigma(p\bar{p} \rightarrow W') \times \mathcal{B}(W' \rightarrow tb)$  is also shown.

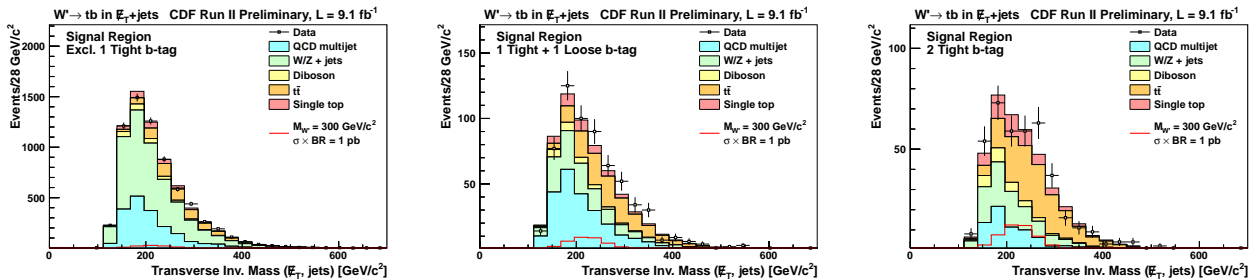


FIG. 2. Distribution of the invariant transverse mass of  $E_T$  and jets in the signal region defined by the QCD Neural Network  $> 0.45$  requirement in the subsample with exactly one tight  $b$ -tagged jet (left), one tight and one loose  $b$ -tagged jet (middle) and two tight  $b$ -tagged jets (right). Templates for background processes are normalized to their expected values. The expected distribution for a  $300 \text{ GeV}/c^2$   $W'$  with  $\sigma(p\bar{p} \rightarrow W') \times \mathcal{B}(W' \rightarrow tb) = 1 \text{ pb}$  is shown as reference.

$M_{W'}$ [GeV/ $c^2$ ]	Expected limit ${}_{-1\sigma}^{+1\sigma}$ [pb]	Observed limit [pb]
200	$5.40^{+3.30}_{-2.47}$	6.69
300	$1.13^{+0.60}_{-0.38}$	1.42
400	$0.70^{+0.33}_{-0.23}$	0.90
500	$0.49^{+0.25}_{-0.16}$	0.53
600	$0.31^{+0.14}_{-0.09}$	0.32
700	$0.22^{+0.10}_{-0.07}$	0.23
800	$0.21^{+0.10}_{-0.06}$	0.22
900	$0.21^{+0.10}_{-0.07}$	0.22

TABLE II. Expected and observed 95% C.L. limits on  $\sigma(p\bar{p} \rightarrow W') \times \mathcal{B}(W' \rightarrow tb)$  as a function of  $W'$  mass  $M_{W'}$ .

## V. LIMITS EXTRACTION

A binned likelihood fit is performed to probe for a  $W' \rightarrow tb$  signal in the presence of SM backgrounds. The likelihood is the product of Poisson probabilities over the bins in the  $M_T(\cancel{E}_T, j_{1,2,3})$  distribution. The mean number of expected events in each bin includes contributions from each background source and from the  $W' \rightarrow tb$  processes assuming a given value of  $M_{W'}$ . The method employed is a Bayesian likelihood method [23] with a flat, non-negative, prior probability for the  $W'$  boson production cross section times branching fraction,  $\sigma(p\bar{p} \rightarrow W') \times \mathcal{B}(W' \rightarrow tb)$ , and truncated Gaussian priors for the uncertainties on the acceptance and shape of the backgrounds. We combine the three  $b$ -tagging regions by taking the product of their likelihoods and simultaneously varying the correlated uncertainties.

Systematic uncertainties considered in the fit include both uncertainties on template normalization, and uncertainties on the shape of the  $M_T(\cancel{E}_T, j_{1,2,3})$  distribution. Uncertainties due to the same source are considered 100% correlated. These uncertainties, which apply to both signal and backgrounds, include luminosity measurement (6%),  $b$ -tagging efficiency (8 to 16%), trigger efficiency (1 to 3%), lepton veto efficiency (2%), parton distribution function (3%), and up to 6% for the jet-energy scale [15]. Initial- and final-state radiation uncertainties (2%) are applied only to top processes ( $t\bar{t}$  and single top).

The uncertainties due to simulations statistics, and the uncertainties on the normalization of  $t\bar{t}$  (6%), single top (15%), diboson (6%) from the theoretical cross-section calculations, and QCD multijet (3 to 10%, calculated from scale factors) are not correlated. The rates of production of events with a  $W$  or a  $Z$  boson plus heavy-flavor jets are associated with 30% uncertainties due to uncertainties in the estimation of the heavy-flavor fraction with respect to the overall  $W/Z + \text{jets}$  contribution. Shapes uncertainties on the  $M_T(\cancel{E}_T, j_{1,2,3})$  distribution obtained by varying the jet-energy scale by  $\pm 1\sigma$  from its central values are associated to all simulated processes. Shapes uncertainties obtained by varying the  $f_i$  probability in each tagging category by  $\pm 1\sigma$  are applied for the QCD multijet templates. An additional uncertainty on the  $b$ -tagging efficiency is applied to signal templates as a  $E_T$ -dependent term, to correctly take into consideration the effect of the extrapolation of the  $b$ -tagging scale factor to the high- $E_T$  regions typical of  $W' \rightarrow tb$  events.

## VI. RESULTS

The aforementioned procedure is carried out for all signal mass hypotheses, obtaining 95% C.L. upper limits on  $\sigma(p\bar{p} \rightarrow W') \times \mathcal{B}(W' \rightarrow tb)$  as a function of  $M_{W'}$ , using the methodology described in Ref. [24]. The expected and observed upper limits are shown in Table II and in Figure 3. The observed limits are compatible with the expectations calculated assuming no  $W' \rightarrow tb$  signal is present in the data. By comparing the limits on  $\sigma(p\bar{p} \rightarrow W') \times \mathcal{B}(W' \rightarrow tb)$  with with the theoretical NLO calculations for a right-handed  $W'$  with SM-like couplings [11], we exclude  $W'$  bosons for masses less than 820 (840) GeV/ $c^2$  in cases where decay to leptons is allowed (forbidden).

For a simple  $s$ -channel model with effective coupling  $g_{W'}$ , the cross-section is proportional to  $g_{W'}^4$ . Relaxing the assumption of universal weak coupling, the limits on the cross-section can be interpreted as upper limits on  $g_{W'}$  as a function of  $M_{W'}$ . The excluded region of the  $g_{W'}-M_{W'}$  plane is shown in Figure 4, with  $g_{W'}$  expressed in units of  $g_{\text{SM}}$ . For a value of  $M_{W'} = 300$  GeV/ $c^2$ , the effective coupling is constrained at the 95% C.L. to be less than 0.4 of the  $W$  boson coupling.

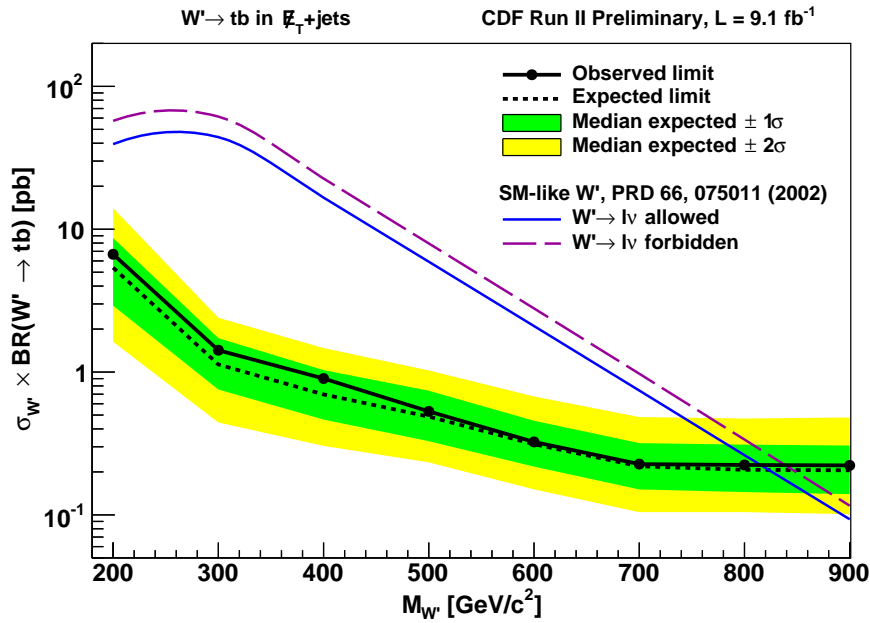


FIG. 3. Observed and expected limits on  $\sigma(p\bar{p} \rightarrow W') \times \mathcal{B}(W' \rightarrow tb)$ , with  $\pm 1\sigma$  and  $\pm 2\sigma$  confidence intervals and theoretical predictions for a right-handed  $W'$  with SM-like couplings in cases where the leptonic decay mode  $W' \rightarrow \ell\nu$  is allowed (solid line) or forbidden (dashed).

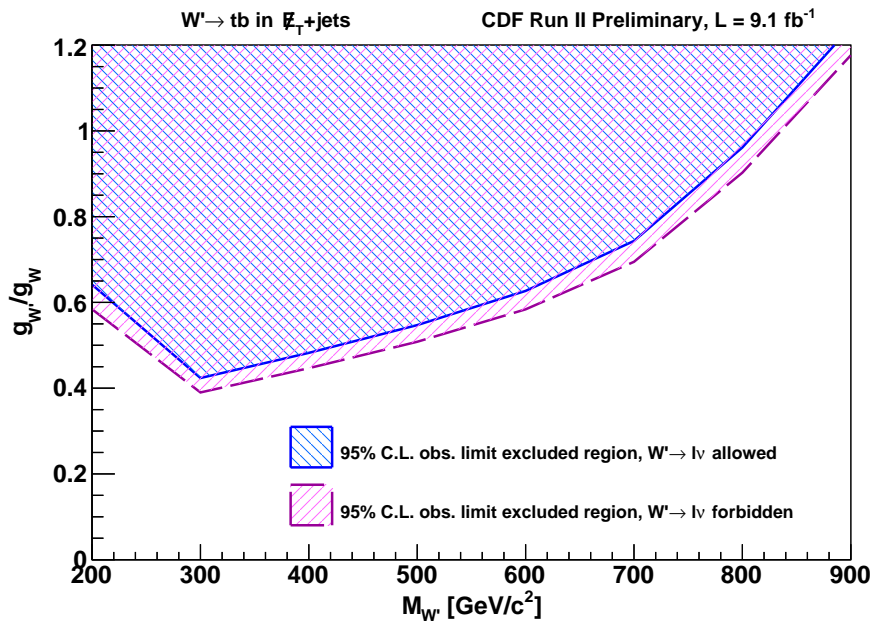


FIG. 4. Observed 95% C.L. limits on the coupling strength of a right-handed  $W'$  compared to the SM  $W$  boson coupling,  $g_{W'}/g_{SM}$ , as a function of  $M_{W'}$  in cases where the leptonic decay mode  $W' \rightarrow \ell\nu$  is allowed or forbidden. The patterned region above each line is excluded.

## VII. SUMMARY

In conclusion, we have performed a search for a massive resonance decaying to  $tb$  in the  $\cancel{E}_T$  plus jets final state with the full CDF II dataset, corresponding to an integrated luminosity of  $9.1 \text{ fb}^{-1}$ . The data are found to be consistent with the background-only hypothesis, and upper limits are set on the production cross-section times branching ratio

at the 95% confidence level. For a specific benchmark model (left-right symmetric SM extension), in cases where the leptonic decay mode is allowed (forbidden), we exclude  $W'$  bosons with masses lower than 820 (840)  $\text{GeV}/c^2$ . For masses smaller than approximately 700  $\text{GeV}/c^2$ , this search yields the most constraining limits to date on narrow  $tb$  resonances production (Figure 5).

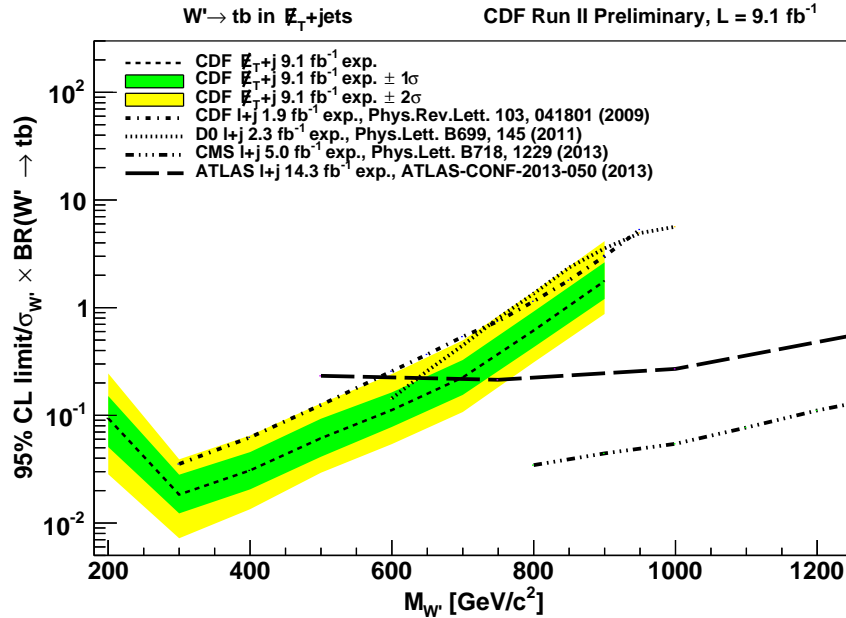


FIG. 5. Comparison of results from this analysis and most recent analyses at the Tevatron and the LHC. To allow a direct comparison, 95% C.L. expected limits have been divided by the theoretical prediction corresponding to the same model for a  $W'$  with SM-like couplings. Results from this analysis are the most sensitive in the mass range below approximately 700  $\text{GeV}/c^2$ .

## ACKNOWLEDGMENTS

We thank the Fermilab staff and the technical staffs of the participating institutions for their vital contributions. This work was supported by the U.S. Department of Energy and National Science Foundation; the Italian Istituto Nazionale di Fisica Nucleare; the Ministry of Education, Culture, Sports, Science and Technology of Japan; the Natural Sciences and Engineering Research Council of Canada; the National Science Council of the Republic of China; the Swiss National Science Foundation; the A.P. Sloan Foundation; the Bundesministerium für Bildung und Forschung, Germany; the Korean World Class University Program, the National Research Foundation of Korea; the Science and Technology Facilities Council and the Royal Society, United Kingdom; the Russian Foundation for Basic Research; the Ministerio de Ciencia e Innovación, and Programa Consolider-Ingenio 2010, Spain; the Slovak R&D Agency; the Academy of Finland; the Australian Research Council (ARC); and the EU community Marie Curie Fellowship Contract No. 302103.

- 
- [1] J. C. Pati and A. Salam, *Phys.Rev.* **D10**, 275 (1974).
  - [2] Y. Mimura and S. Nandi, *Phys.Lett.* **B538**, 406 (2002), arXiv:hep-ph/0203126 [hep-ph].
  - [3] G. Burdman, B. A. Dobrescu, and E. Ponton, *Phys.Rev.* **D74**, 075008 (2006), arXiv:hep-ph/0601186 [hep-ph].
  - [4] H. Georgi, E. E. Jenkins, and E. H. Simmons, *Nucl.Phys.* **B331**, 541 (1990).
  - [5] E. Malkawi, T. M. Tait, and C. Yuan, *Phys.Lett.* **B385**, 304 (1996), arXiv:hep-ph/9603349 [hep-ph].
  - [6] M. Perelstein, *Prog.Part.Nucl.Phys.* **58**, 247 (2007), arXiv:hep-ph/0512128 [hep-ph].
  - [7] T. Aaltonen *et al.* (CDF Collaboration), *Phys.Rev.Lett.* **103**, 041801 (2009), arXiv:0902.3276 [hep-ex].
  - [8] V. M. Abazov *et al.* (D0 Collaboration), *Phys.Lett.* **B699**, 145 (2011), arXiv:1101.0806 [hep-ex].
  - [9] G. Aad *et al.* (ATLAS Collaboration), *Phys.Rev.Lett.* **109**, 081801 (2012), arXiv:1205.1016 [hep-ex].

- [10] S. Chatrchyan *et al.* (CMS Collaboration), *Phys.Lett.* **B718**, 1229 (2013), arXiv:1208.0956 [hep-ex].
- [11] Z. Sullivan, *Phys. Rev. D* **66**, 075011 (2002).
- [12] D. Acosta *et al.* (CDF Collaboration), *Phys.Rev.* **D71**, 032001 (2005), arXiv:hep-ex/0412071 [hep-ex].
- [13] D. Acosta *et al.* (CDF Collaboration), *Phys.Rev.* **D71**, 052002 (2005), arXiv:hep-ex/0411059 [hep-ex].
- [14] T. Aaltonen *et al.* (CDF Collaboration), *Phys.Rev.Lett.* **109**, 111805 (2012), arXiv:1207.1711 [hep-ex].
- [15] A. Bhatti *et al.* (CDF Collaboration), *Nucl.Instrum.Meth.* **A566**, 375 (2006), arXiv:hep-ex/0510047 [hep-ex].
- [16] A. Abulencia *et al.* (CDF Collaboration), *Phys.Rev.* **D74**, 072006 (2006), arXiv:hep-ex/0607035 [hep-ex].
- [17] M. L. Mangano, M. Moretti, F. Piccinini, R. Pittau, and A. D. Polosa, *JHEP* **0307**, 001 (2003), arXiv:hep-ph/0206293 [hep-ph].
- [18] S. Alioli, P. Nason, C. Oleari, and E. Re, *JHEP* **1006**, 043 (2010), arXiv:1002.2581 [hep-ph].
- [19] T. Sjostrand, S. Mrenna, and P. Z. Skands, *JHEP* **0605**, 026 (2006), arXiv:hep-ph/0603175 [hep-ph].
- [20] R. Brun, F. Carminati, and S. Giani, *CERN* **W5013** (1994).
- [21] M. Bentivegna, Q. Liu, F. Margaroli, and K. Potamianos, (2012), arXiv:1205.4470 [hep-ex].
- [22] The event sphericity is defined by  $S = \frac{3}{2}(\lambda_2 + \lambda_3)$ , where the sphericity tensor is  $S^{\alpha\beta} = (\sum_i p_i^\alpha p_i^\beta) / (\sum_i p_i^2)$  and  $\lambda_1 > \lambda_2 > \lambda_3$  are its three eigenvalues and satisfy  $\lambda_1 + \lambda_2 + \lambda_3 = 1$ . The index  $i$  refers to each jet in the event.
- [23] K. Nakamura *et al.* (Particle Data Group), *J.Phys.* **G37**, 075021 (2010).
- [24] T. Aaltonen *et al.* (CDF Collaboration), *Phys.Rev.* **D82**, 112005 (2010), arXiv:1004.1181 [hep-ex].